Mon. Not. R. Astron. Soc. **301,** 941–954 (1998)

On the unusual activity of the Perseid meteor shower (1989–96) and the dust trail of comet 109P/Swift–Tuttle

P. Jenniskens,[1★†] H. Betlem,[2‡] M. de Lignie,[2] C. ter Kuile,[2] M. C. A. van Vliet,[2] J. van 't Leven,[2] M. Koop,[3] E. Morales[3] and T. Rice[3]

[1] *NASA/Ames Research Center, Mail Stop 239–4, Moffett Field, CA 94035–1000, USA*
[2] *Dutch Meteor Society, Lederkarper 4, NL-2318 NB Leiden, the Netherlands*
[3] *California Meteor Society, 1037 Wunderlich Drive, San José, CA 95129–3159, USA*

Accepted 1998 July 30. Received 1998 July 14; in original form 1998 March 17

ABSTRACT

We present the first measurements of the radiant and orbit of meteoroids that are part of the unusual Perseid activity called the 'Perseid Filament'. This filament was encountered by Earth in the years before and after the return of the comet to perihelion in December of 1992. Between 1989 and 1996, there were brief meteor outbursts of near-constant duration with a symmetric activity profile. In 1993, however, rates increased more gradually to the peak. That gradual increase is identified here as a separate dust component, which we call the 'Nodal Blanket'. We find that the Nodal Blanket has a very small radiant dispersion. On the other hand, the Perseid Filament has a radiant that is significantly dispersed and systematically displaced by 0.3°. This dispersion implies that unusually high ejection velocities or planetary perturbations must have had time to disperse the stream. In both cases, one would expect a rapid dispersion of matter along the comet orbit. In order to explain the concentration of dust near the comet position, we propose a novel scenario involving long-term accumulation in combination with protection of the region near the comet against close encounters with Jupiter due to librations of the comet orbit around the 1:11 mean-motion resonance.

Key words: comets: individual: 109P/Swift–Tuttle – meteors, meteoroids – Solar system: general.

1 INTRODUCTION

Most of the mass that comets lose in the form of dust is shed as relatively large grains for which β, the ratio of solar radiation pressure forces over solar gravity forces, is constrained by $\beta > 10^{-2}$. Those grains stay close to the comet nucleus initially, but will disperse along the comet path after one orbit because the ejection velocity affects their orbital period (Plavec 1955). The resulting dust trails have been detected in the orbits of short-period comets in mid-infrared (mid-IR) images taken with *IRAS* (Davies et al. 1984; Sykes et al. 1986) and recently also from *ISO* mid-IR data (Davies et al. 1997).

When grains of that size enter the Earth's atmosphere, they produce visual and telescopic meteors. Shortly after the discovery of dust trails, it was realized that meteor storms, and meteor outbursts in general, may be caused by the Earth encountering low-density extensions of these dust trails (Kresák 1993; Jenniskens 1995). Hence, it should be possible to derive fundamental parameters such as the ejection velocities, the particle mass-to-surface ratio and the particle size distribution from Earth-based observations of these meteor outbursts.

The Perseid meteor shower is caused by debris of comet 109P/Swift–Tuttle, a comet of 1P/Halley type, the meteoroids of which radiate from the constellation of Perseus. The normal annual Perseid shower is particularly strong and well-observed, with peak zenith hourly rate ZHR = 84 ± 5 meteor h^{-1}. It takes Earth 2.5 d to pass the central portion of the stream. The meteor rate variation along the Earth's path has been measured well (e.g. Denning 1898; Mason & Sharp 1981; Zvolankova 1984; Lindblad & Simek 1986; Jenniskens 1994a).

Many studies of Perseid activity have suggested large year-to-year variations in the peak flux of the annual shower and multiple maxima (see references in Kronk 1988). However, those studies that carefully consider instrumental effects and statistical errors tend to find that the peak annual rate varies by only 20 per cent or so, with no significant changes over a smooth and featureless activity profile (Jenniskens 1994a). Until 1989, incidental reports of much higher activity could be dismissed by better than usual observing conditions, differences in perception, etc. (e.g. Jenniskens 1992).

Unusual activity of the Perseid shower has been confirmed only

★E-mail: peter@max.arc.nasa.gov
† Associated with the SETI Institute.
‡ Guest observer at Leiden Observatory.

for the years around the return of the comet to perihelion, which happened most recently in 1992 December. Roggemans' (1989) detection of a brief increase of rates during the 1988 return has often been credited as the first sign of this unusual activity, but this result has remained in doubt. Another peak at a somewhat different time was noticed in the global analysis of 1989 Perseid counts by Koschack & Roggemans (1991). In hindsight, this was the first detection of a Perseid outburst: a significant increase over annual rates.

The unusual Perseid activity was established only during the 1991 outburst by Japanese amateur observers from the Shinshu University Astro OB Club, who obtained impressive photographs showing numerous trails (Taguchi 1991; Marsden 1991). 11 Perseids were photographed from two or more sites that were far enough apart for triangulation, from which the direction of the meteor trajectory in the atmosphere (the radiant) was derived. Shiba, Ohtsuka & Watanabe (1993) measured seven radiants clustering in a 0.1° region at the coordinates RA = 46.1, Dec. =+57.5 (J2000). In the following years, meteor outbursts continued to occur, while Lindblad & Porubcan (1994) traced the outbursts at a very low intensity back to the 1960s from a slight increase in the rate of photographic records.

The repetitive recurrence of the Perseid outbursts invited a proactive observing strategy, i.e. travelling to a clear and dark location with a favourable radiant position at the expected time of the outburst. This is necessary, because the meteor outbursts are visible only from about a quarter of the Earth's surface. Moreover, outbursts in subsequent years are seen from a different continent, because of the leap-year misfit in the number of days in a year.

In a series of such efforts, we applied visual and photographic techniques to measure the variation in meteoroid flux along the path of comet 109P/Swift–Tuttle, the width of the dispersed debris in the Earth's path and the particle size distribution. In addition, we obtained the first meteoroid orbits of outburst Perseids. These measurements have now been reduced and the results are presented here.

2 OBSERVATIONS

Successive observing campaigns were held in the Swiss Jura and French Vozges mountains in 1992, the French Haute Provence in 1993, the San Francisco Bay Area of California in 1994 and near Hannover in Germany in 1996. A network of small 35-mm (focal length 50 mm, f/1.8) cameras was deployed for triangulation of meteor trajectories and the calculation of meteoroid orbits. These efforts were supported by a team of visual observers who provided Perseid counts and the time of bright meteors. The observing technique is described in Betlem et al. (1998). During our first attempt in 1992 the outburst was mostly lost in evening twilight (Marsden 1992; Betlem et al. 1992), and the 1996 campaign suffered from bad weather. Here, we report on the highly successful 1993 and 1994 campaigns, adding Perseid rates from our campaigns of 1992 and 1996.

The first successful campaign in 1993 consisted of four stations near the towns of Puimichel, Tourves, Rognes and Lardiers in the south of France. The camera platforms were operated by members of the Dutch Meteor Society (DMS). The second campaign in 1994 was made possible by meteor observers of the Fremont Peak Observatory Association and San Jose Astronomical Association of California, who are now the California Meteor Society. Platforms were located near Los Banos, Fremont Peak State Park, Henry Coe State Park and Holler Observatory in the hills behind Lick Observatory (Jenniskens 1994b). A small number of additional photographs was obtained by other amateur observers in the region. The technique was the same as in 1993 and the data were reduced in the same way, described in Betlem et al. (1998).

3 RESULTS: FLUX AND PARTICLE SIZE DISTRIBUTIONS

3.1 The Perseid Filament

A picture has gradually emerged with each report on the peak flux, the time of maximum, the shape of the meteor activity curve and the meteor magnitude distribution. Each successive Perseid return mapped out the dust distribution along the comet path before and after the comet, inside the comet orbit at a distance of about 0.0009 au, which was the minimum distance between the comet and Earth's orbit during the 1992 return of comet 109P/Swift–Tuttle.

During each return since 1989, a brief increase of Perseid rates was detected (the meteor outburst), which varied in intensity from year to year and was all but absent before 1989. Fig. 1 shows the variation of meteor fluxes (in terms of ZHR) as a function of the position of the Earth in its orbit in terms of solar longitude λ_0 (epoch J2000). Small dots show our rates calculated from the 1993 DMS observations by van Vliet (1993, 1994) and similar results from the 1992, 1994 and 1996 observations.

These results are in good agreement with data by Brown & Rendtel (1997), with an update by Rendtel & Arlt (1996), shown as larger black dots in Fig. 1. These data were obtained from an international exchange of visual observations. The reported rates by Brown & Rendtel were corrected by + 15 per cent in order to match the ZHR scale of Jenniskens (1994a) and corresponding conversion to mass influx.

Not all years provided the same coverage and level of accuracy. Notably, the results of 1990, 1992 and 1995 are hampered by moonlight, while those of 1996 were hampered by clouds. To further define the shape of the activity curves, we have included individual ZHRs (•) in sparsely sampled years, and radio forward-scatter and radar back-scatter data (+) that were background-subtracted and scaled to the visual data through multiplication by a constant scaling factor.

We find no systematic differences in the width of the flux profiles between visual and radio or radar data, probably because these techniques detect Perseids of similar brightness to those seen by the visual observers (about magnitude + 3). However, we also find no difference in the duration of the shower for relatively bright (about – 1 mag) photographic meteors obtained during the 1994 campaign (Fig. 1 – ○). These photographic meteors are caused by particles of typically $\beta = 3 \times 10^{-4}$, while visual meteors have about $\beta = 2 \times 10^{-3}$. In the classical models of dust grain ejection, the ejection velocity scales with $V_{ej} \sim \sqrt{\beta}$, and the duration of the outbursts is expected to scale with V_{ej} if caused by the ejection process. Hence, the outbursts should be a factor of 2.6 narrower for the photographic meteors. On the contrary, the observations point to a difference in width of less than 50 per cent, implying that other effects add to the width of the outburst.

We found that the duration of the meteor outbursts varied little from year to year, with a notable exception in 1993 (Section 3.2). This is demonstrated by superposing on the ZHR data a curve of constant width and a shape of the form (Jenniskens 1995):

$$\mathrm{ZHR} = \mathrm{ZHR}_{\max} \times 10^{-B\,|\,\lambda_0 - \lambda_0^{\max}\,|}, \qquad (1)$$

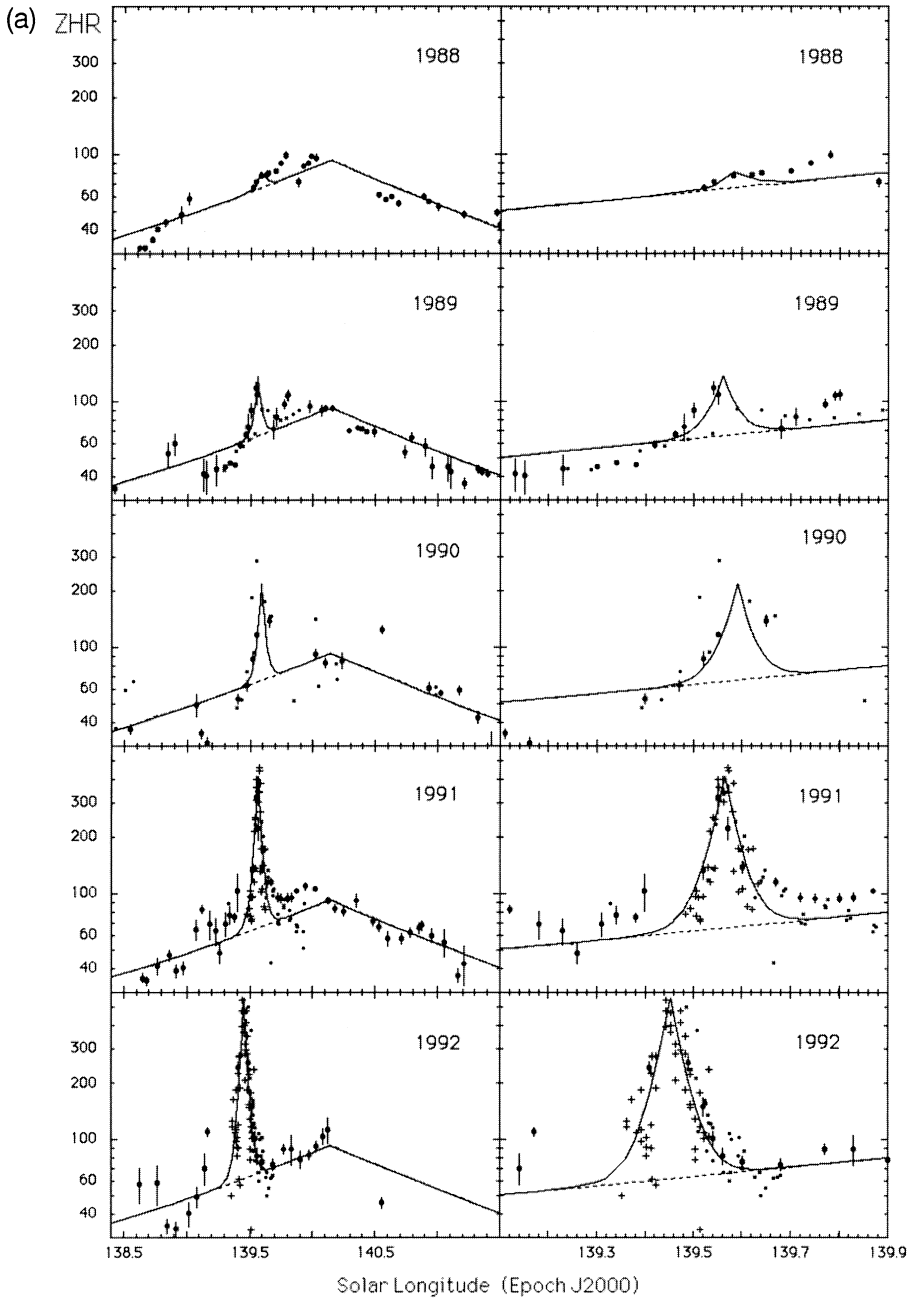

Figure 1. Meteor stream activity curves of the Perseid shower in the period prior to passage of the comet by perihelion in 1992 December. *Notes to Fig. 1(a):* Large dots: data by Brown & Rendtel (1997), scaled upwards by 15 per cent to match the ZHR scale of Jenniskens (1994a). Data for 1990 scaled upward to match annual stream activity. Small dots: 1989: visual data by Koschack & Roggemans (1991); 1990: visual observations by Michael Morrow, Phyllis Eide & David Swann, USA, Peter Brown, Canada; 1991: visual observations from Yasuo Yabu, Japan (Roggemans, Gijssens & Rendtel 1991). Crosses: radar data by Watanabe et al. (1992) and forward-scatter data by Shimoda, Suzuki & Maeda (1993). Forward-scatter counts were background-subtracted and scaled by a constant scaling factor to match visual observations. 1992: Visual observations by Chinese observers Chen Wu and Ouyang Tianjing (Pin-Xin 1992) and Czech observers I. Micek, T. Nasku, J. Kysely (Brown, Gijssens & Rendtel 1992; Znojil 1992), in addition to visual observations by members of the Dutch Meteor Society: M. Langbroek, M. van Vliet, C. Johannink, A. Scholten, A. Jenniskens, P. Jenniskens (van Vliet 1993). Crosses: radio-MS data by Shimoda et al. (1992). *Notes to Fig. 1(b):* Large dots are data by Brown & Rendtel (1997) and Rendtel & Arlt (1996). Individual returns: 1993: small dots are visual observations by DMS observers (Van Vliet 1994); 1994: small dots are visual observations from Californian observers D. Holman, P. Jenniskens, A. Knöfel, Ken Lakins, L. Nelson, I. Rendtel, J. Rendtel, I. Rice, R. Thompson (Jenniskens 1994b), also A. Kimble, G. Zentz, G. Williams from Florida, and J. Shalamskas from Hawaii. Open circles are the rate of photographed meteors. 1996: small dots are visual observations by 13 observers of the Dutch Meteor Society from a location in Germany. Crosses are forward-scatter counts by I. Yrjölä from Finland, background-subtracted, corrected for observability and fitted to the annual curve using a constant scaling factor (Yrjölä & Jenniskens 1998).

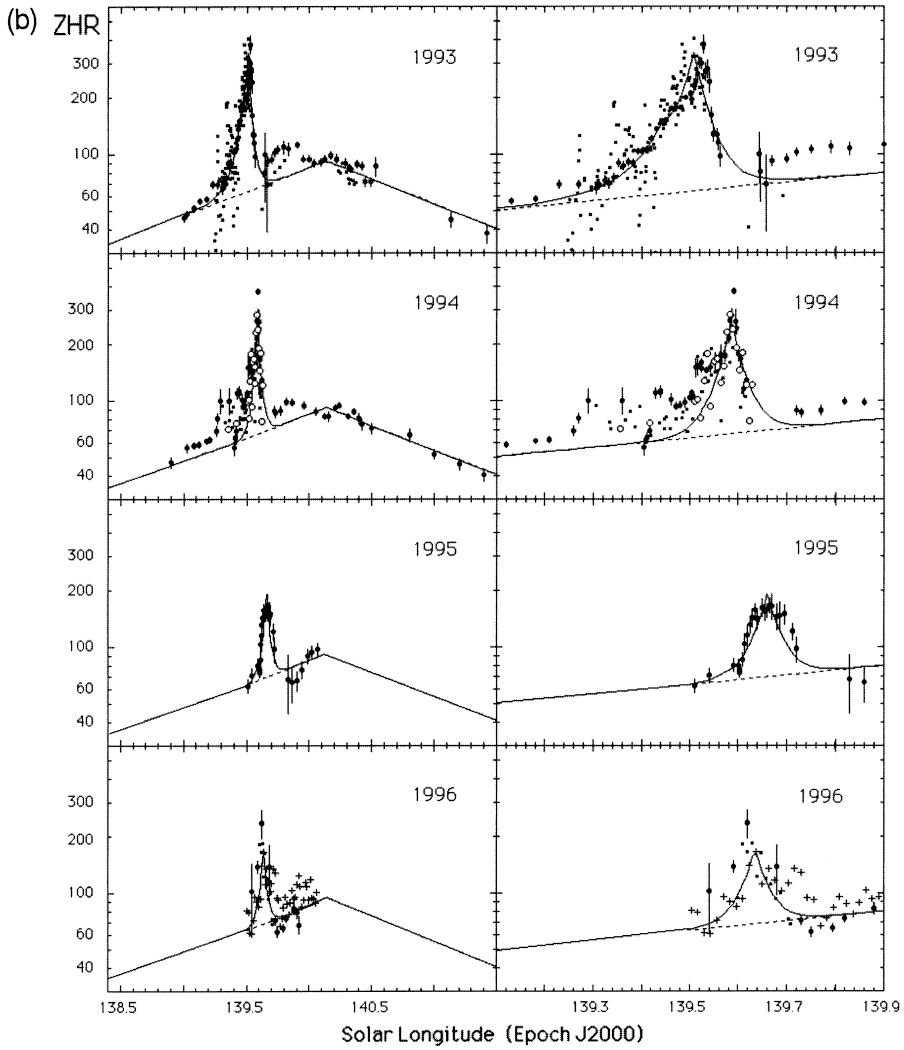

Figure 1 – *continued*

with constant B but varying peak time $\lambda_0{}^{\max}$ and peak activity ZHR_{max}. For the annual Perseid stream background, we adopted the mean curve derived by Jenniskens (1994a) from observations in the period 1981–91. The observed outburst profiles (Fig. 1) are well-described by equation (1), with a constant $B = 15 \pm 3$, making the equivalent duration of these outbursts a mere 1.4 h (as compared to 2.5 d for the annual shower), whereby the equivalent duration is defined as the duration of a block-shaped profile with the same peak intensity and integrated flux profile.

Each year, the peak time and peak activity varied. Values of $\lambda_0{}^{\max}$ and ZHR_{max} are given in Table 1 and the variation from year to year is shown in Fig. 2. Before perihelion passage, the time of maximum shifted towards the comet node at $\lambda_0 = 139.445$ (Yau, Yeomans & Weissman 1994), as reported by Brown & Rendtel (1997), while after perihelion passage the node shifted back to the asymptotic value obtained from excess photographed Perseids tens of years prior to perihelion (Lindblad & Porubcan 1994), marked by an arrow in Fig. 2. We note that this pattern has been reported for other series of near-comet-type meteor outbursts as well (Jenniskens 1995), and an early recognition gave us the guidance needed to see a glimpse of the 1992 outburst (Langbroek & Jenniskens 1992; Betlem et al. 1992). The early 1988 detection by Roggemans (1989) does not fit well in the gradual sequence of events and is dismissed as resulting from improperly corrected differences in observing techniques on different continents.

The level of peak activity is most sensitive to uncertain corrections for observing conditions and varies somewhat between our analysis and that of Brown & Rendtel (1997). We find a more gradual change from year to year, with most activity confined to the period 1989–96 (Fig. 2, lower panel). The rate of increase is best described in a plot of the log (ZHR_{max}) versus year. A linear fit (an exponential increase as in equation 1) gives a value of $B = -0.36\,\mathrm{yr}^{-1}$ before perihelion and $B = -0.23\,\mathrm{yr}^{-1}$ after perihelion. Hence, the equivalent period of time that the trail took to pass the Earth, the extent along the comet orbit, is 3.1 yr or 1/44th of the orbital period.

The duration of the outbursts and extent along the comet orbit define two of three dimensions of the dust structure. Reports of a meteor outburst during the previous return in 1862 at about the same intensity (Nogami 1995; Jenniskens 1995), at a time when the comet orbit passed 0.0046 au inside Earth's orbit, imply that the stream extends inwards from the comet orbit at least some 0.0037 au. This defines the relative size of this structure: 0.0010 ± 0.0002 au thick, at least 0.004 au wide and several au long (a time span of 3.1 yr at the node of the comet orbit).

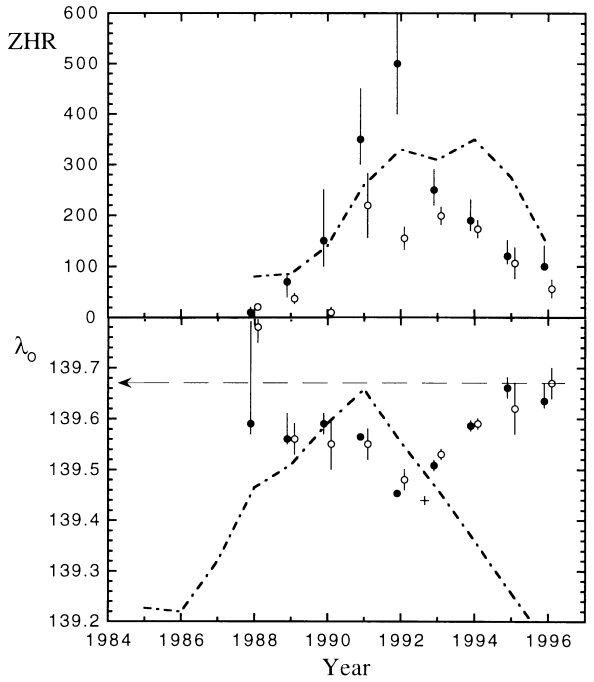

Figure 2. The position of the time of maximum and the peak rate for the Perseid outbursts in the period 1988–96. Dotted and dash–dotted lines show model calculations presented in this paper and model calculations by Williams & Wu (1994), respectively.

The relatively brief and near-constant duration of the outbursts implies that the Earth crossed a ribbon-like structure of dust, which is extended more in the plane of the comet orbit than perpendicular to it, and extends much further along the comet orbit. In referring to this component, we will adopt the name Perseid Filament', following Lindblad & Porubcan (1994).

The particle size distribution in this structure has not varied significantly from year to year (Table 2). We confirm that the relative number in successive magnitude intervals (χ) was less during the outbursts than for the annual stream activity (Rendtel 1993; Brown & Rendtel 1997); hence the outbursts were rich in bright meteors. The measured values imply a mass distribution index $s\,(=1+2.5\ \log\ \chi)=1.73\pm0.04$ as opposed to $s=2.3$ for sporadic meteors in the same mass range. The absence of a change in this ratio after perihelion passage is surprising, because models predict a steeper distribution (higher χ) behind the comet orbit, as a result of radiation pressure (Kresák 1976). In fact, no such change is observed.

From the measured peak fluxes and meteor brightness distributions, we can estimate the total mass of matter in the Perseid Filament, assuming a constant magnitude distribution index over the mass range 10^{-6}–10^{2} g (Jenniskens 1994a). The estimate depends most severely on the assumption made about the dispersion of matter in the plane of the comet orbit which, as said, extends inwards from at least 0.0009–0.0046 au and may also extend outwards. Assuming an exponential decay of dust peaking at the orbital position near the comet with an equivalent width of 0.0037 au, we have a lower limit of $M>3\ 10^{14}$ g for the Perseid Filament. This compares with $M=5\ 10^{16}$ g for the annual stream component calculated in the same manner (Jenniskens 1994a). The masses of dust trails in the

Table 1. The position, peak activity, and duration of the Perseids. Parameters refer to equation (1).

Year	$\lambda_{\odot}$ (J2000) (deg.)	ZHR_{max} (hr.$^{-1}$)	B (deg.$^{-1}$)	$\lambda_{\odot}$ (J2000) (deg.)	ZHR_{max} (hr.$^{-1}$)	B (deg.$^{-1}$)	ref.
1950-1979	-.-	<6	-.-	139.67±0.05	-.-	-.-	[1]
1988	139.59 +0.2,-0.02	<20	-.-	139.78±0.03	21±4	-.-	[2]
1989	139.56 +0.05,-0.01	70 +10,-20	~15	139.56±0.03	37±10	-.-	[2]
1990	139.57 ±0.02	150 +100,-50	~15	139.55±0.05	10±10	-.-	[2]
1991	139.564±0.005	350 +100,-50	19±4	139.55±0.03	219±63	-.-	[2]
				139.566	500±100	25±7	[3]
1992	139.453±0.005	550 +200,-100	12±3	139.48±0.02	155±22	-.-	[2]
				139.168	400±50	22±4	[3]
1993	139.508±0.01	250 +40,-30	~15	139.53±0.01	199±17	-.-	[2]
				139.507	230±30	-.-	[3]
1994	139.586±0.01	190 +40,-20	15±3	139.59±0.01	173±17	-.-	[2]
1995	139.66 ±0.02	120, +30, -15	16±2	139.62±0.05	106±30	-.-	[4]
1996	139.64+0.03,-0.02	100 ±40	11±3	139.67±0.03	56±17	-.-	[4]

[1] Lindblad & Porubcan (1994).
[2] Brown & Rendtel (1997).
[3] Jenniskens (1995).
[4] Rendtel & Arlt (1996).

Table 2. The meteor brightness distribution of the various dust components.

Year	χ Filament (a)	(b)	χ Nodal Blanket (a)	(b)	χ annual (a)	Ref.	Technique
pre-perihelion:							
1991	1.86-2.14	1.7	-.-	-.-	2.4-3.1	[2]	visual
	1.67±0.06	1.6	-.-	-.-	2.17±0.06	[3]	radar under-d
	1.17±0.01	1.2	-.-	-.-	1.25±0.02	[3]	radar over-d
1992	2.12±0.15	1.7	-.-	-.-	2.5±0.2	[1]	visual
	1.75-1.98	1.6	-.-	-.-	1.90-2.65	[2]	visual
	1.96±0.24	1.6	-.-	-.-	2.3±0.1	[4]	visual
post-perihelion:							
1993	2.02±0.04	1.9	1.72±0.02	1.5	2.27±0.01	[1]	visual
	~1.58	1.5	-.-	-.-	2.3±0.3	[1]	photo
	1.92±0.03	1.9	1.87±0.03	1.7	2.05±0.05	[5]	visual
	1.79±0.05	1.7	1.85±0.03	1.7	2.00±0.09	[6]	visual
1994	1.9±0.2	1.7	-.-	-.-	~2.5	[1]	visual
	1.8±0.3	1.7	-.-	-.-	2.3±0.3	[1]	photo
	1.82±0.05	1.7	-.-	-.-	1.90±0.05	[5]	visual

[1] This work.
[2] Grishchenyuk (1993).
[3] Watanabe et al. (1992).
[4] Znojil (1992).
[5] Brown & Rendtel (1997).
[6] Rendtel (1993).

orbits of short-period comets are of order 10^{12-14} g (Sykes & Walker 1992).

3.2 The 1993 Perseid Nodal Blanket

In 1993, Perseid activity was surprisingly high in the hours leading up to the main outburst. Our initial interpretation was that the sheet was broader after perihelion than before (Jenniskens 1995), an effect that was predicted in some models of stream formation.

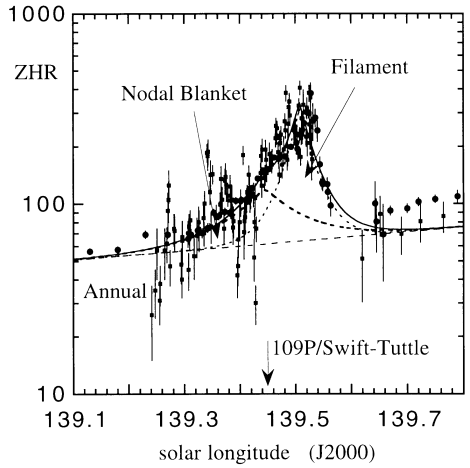

Figure 3. 1993 Perseid activity curve (fragment of Fig. 1) with schematic representation of the Nodal Blanket, Perseid Filament and annual stream components (dashed lines).

However, that conclusion is incorrect. After including post-outburst observations by US observers and observations in later years, we conclude that the profile in 1993 was asymmetric, with an unusually gradual increase followed by a normal fast decrease of rates. This feature was pointed out by Brown & Rendtel (1997) and is confirmed by our observations, although the details of the activity curve at the peak vary. These discrepancies are caused by different corrections for moonlight and twilight for European observers, as well as ill-matched contributions from European observers (high radiant position) and US observers (low radiant position) at the time of the peak.

One of us first suggested that a separate dust component was responsible for the gradual increase of rates in 1993 (Van Vliet 1994). When we align a $B = 15$ profile (equation 1) with the descending branch of the activity curve, then the remaining part can be fitted well with a similar profile with $B = 6 \pm 1$ and $\mathrm{ZHR}_{\max} = 80 \pm 20$, if we assume that $\lambda_0^{\max} = 139.445$ at the node of 109P/Swift–Tuttle. This decomposition is illustrated in Fig. 3.

Here, we will refer to this component in the activity curve as the 'Nodal Blanket', for lack of a better name (perhaps 'Resonant Debris Blanket' would be better – see Section 5), because it is found at the present node of the comet orbit and is thicker than the Filament. The Nodal Blanket was encountered in 1993, and perhaps again in 1994. If we made the naive assumption that the Nodal Blanket is dispersed in the plane of the comet orbit in the same way as the Filament, and the peak dust density is that measured in 1993, then its total mass would be a factor of 10 smaller than that of the Perseid Filament.

The Filament and Nodal Blanket are the only significant structures in the meteor outburst profiles on top of the annual shower

activity. We do not confirm the further substructure suggested in Brown & Rendtel (1997).

4 RESULTS: VELOCITY AND VELOCITY DISPERSION

4.1 Tally of photographic orbits

Further information about the dynamics of these structures can be obtained from a comparison of individual meteoroid orbits. On the night of 1993 August 12, we succeeded for the first time in triangulating outburst meteoroids in a dedicated effort. A total of 95 meteor orbits was measured by the small camera network (Langbroek 1993; de Lignie 1993). Unfortunately, as many as 52 had to be rejected for further analysis because the convergence angle was too small ($Q < 20°$), introducing large uncertainty. The convergence angle is the angle between the two planes through observer and meteor path in the triangulation. Four other orbits were rejected because the time of the meteor is uncertain (DMS 93182, 230, 245 and 269), causing a potential error of 0.5° or more in the RA of the radiant. The remaining 39 radiants and speeds are listed in Table 3(a). An additional eight annual Perseids were measured in the nights before and after the outburst.

In addition, 47 radiant positions were measured on the night of 1994 August 12, but only 14 have good convergence angles $Q > 20°$ (Table 3b). 10 of these provide information on the meteor speed, from which the orbital elements are calculated. Most of these are annual Perseids because of technical problems with the rotating shutters at the time of the outburst. An additional seven annual Perseids were photographed on the next night. The measured radiant and speed of outburst Perseids are listed in Tables 3(a) (1993 data) and 3(b) (1994 data) and are corrected for effects caused by the Earth's gravity.

4.2 The radiant and speed

We find that the outburst meteors have a much smaller dispersion in radiant position than the annual Perseid shower meteors. Fig. 4 shows the radiant distribution after correction for the changing direction of the Earth's motion to that at the position $\lambda_0 = 139.5$ according to

$$\begin{aligned} \mathrm{RA}_{139.5} &= \mathrm{RA}_{\mathrm{geo}} + 1.36(139.5 - \lambda_0), \\ \mathrm{Dec.}_{139.5} &= \mathrm{Dec.}_{\mathrm{geo}} + 0.28(139.5 - \lambda_0). \end{aligned} \quad (2)$$

The results from 1993/94 are shown next to a sample of annual Perseids that were measured by the same techniques at times in the range $\lambda_0 = 138.0$–142.0 in the years from 1981 to 1995, excluding the period of outbursts (Betlem et al. 1998).

It is clear that a significant fraction of the 39 meteors in Table 3 photographed on 1993 August 12 is from the outburst dust component. The rate of annual Perseids detected by the same systems on the next night suggests that only six out of 39 are annual Perseids. Coincidentally, only six radiants are outside the fairly narrow region $45.0° < \mathrm{RA}_{139.5} < 47.5°$ and $57.0° < \mathrm{Dec.}_{139.5} < 58.3°$, and these are marked 'a' for 'annual' in Table 3(a). All others are presumably part of the outburst.

The distribution of speeds is also slightly more narrow than that of the annual Perseid meteors. A preponderance of heliocentric velocities V_h are within the observational error of the value expected for particles with an orbital period similar to that of 109P/Swift–Tuttle: $V_\mathrm{h} = 41.43\,\mathrm{km\,s^{-1}}$ (Fig. 5).

Fig. 6 makes a distinction between the Nodal Blanket and the Perseid Filament. The 1993 Perseids prior to $\lambda_0 = 139.46$ (where the Nodal Blanket dominates – Fig. 3) are marked by solid circles and those after $\lambda_0 = 139.46$ (the Perseid Filament) are marked by circled dots. Also shown are data for the 1994 outburst (open circles) and the 1991 radiants measured by Shiba et al. (1993) (open diamonds). All open symbols refer to the Perseid Filament, although a few may result from the underlying annual stream component.

We find that radiants photographed before $\lambda_0 = 139.46$ on 1993 August 12 (possible members of the Nodal Blanket) are mostly concentrated in a tight cluster. Seven out of 15 radiants cluster in a compact radiant near $\mathrm{RA}_{139.5} = 45.88° \pm 0.08°$, $\mathrm{Dec.}_{139.5} = 57.84° \pm 0.03°$. These are marked '*' in Table 3(a). The radiants have a dispersion of $\pm 0.08°$ in the plane of the comet orbit and $\pm 0.02°$ perpendicular to that (or $\pm 0.08°$ and $\pm 0.05°$ before correction to the same node of 139.5°). The measurement error amounts to about $\pm 0.03°$ in RA and $\pm 0.02°$ in Dec., but varies from orbit to orbit. The velocities measured for these seven radiants are $V_\mathrm{h} = 41.68 \pm 0.15$ (1σ) $\mathrm{km\,s^{-1}}$, close to the expected heliocentric velocity for 109P/Swift–Tuttle. The measurement error of 0.1–$0.5\,\mathrm{km\,s^{-1}}$ can account for the observed dispersion, but not in the case of the annual Perseid shower (Fig. 5).

We find that the radiants after solar longitude 139.460 (dominated by the Filament) are systematically displaced to higher $\mathrm{RA}_{139.5}$ and lower $\mathrm{Dec.}_{139.5}$ compared with the cluster of seven

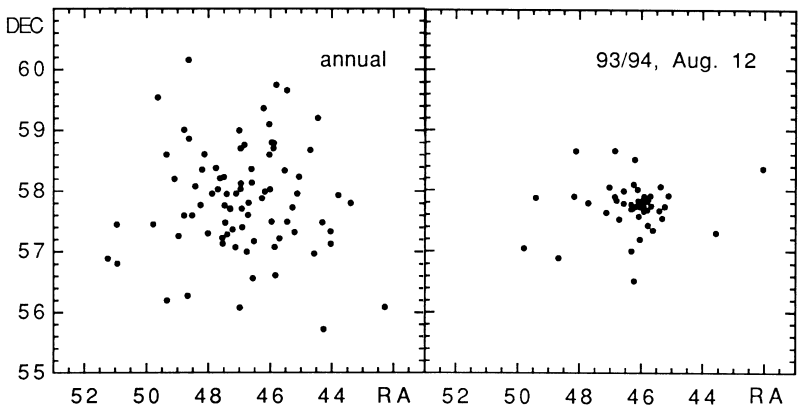

Figure 4. Plot comparing the radiant positions measured on 1993 August 12 and 1994 with those of annual Perseids photographed by similar techniques in 1981–95. The radiants are corrected for the daily motion by theoretical values of $\Delta\mathrm{RA} = +1.36°$ and $\Delta\mathrm{Dec.} = +0.28°$ per degree of solar longitude.

Table 3. (a) Radiant and speed of photographed Perseids during the outburst in 1993 (all data with $Q > 20°$). Columns list the time of the meteor (in solar longitude J2000), absolute brightness at 100 km distance, geocentric velocity (V_g), heliocentric velocity (V_h), formal error, geocentric radiant (right ascension and formal error, declination and formal error), convergence angle (Q), mass-to-surface ratio ($m/C_d S$), and a classification according to: *: cluster of 7 in Perseid Nodal Blanket, +: Filament, a: annual component.

#	Ω (J2000) (deg.)	M_v (magn.)	V_g	V_h (km/s)	±	RA_{geo} (deg.)	±	DEC_{geo} (deg.)	±	Q (deg.)	m/C_dS (g/cm^2)	Class.
August 12, 1993:												
93113	139.2743	-3	59.3	41.2	0.3	45.31	0.00	57.28	0.00	23	0.07	
93118	139.3374	0	60.1	42.2	1.0	46.35	0.15	57.94	0.11	27	-.-	
93122	139.3428	-5	59.1	41.2	0.5	47.96	0.08	57.85	0.03	85	0.34	a
93123	139.3453	-3	59.4	41.5	0.5	45.58	0.26	57.83	0.21	60	0.03	*
93125	139.3586	-5	59.7	41.6	0.3	45.13	0.10	57.50	0.05	65	0.17	
93133	139.3829	0	59.5	41.0	0.5	46.07	-.-	56.48	-.-	28	0.05	a
93134	139.3835	-2	59.0	41.1	0.2	45.89	0.07	57.76	0.02	30	0.15	
93142	139.3964	-7	59.4	41.5	0.1	45.80	0.06	57.81	0.02	60	0.18	*
93143	139.4002	0	59.3	41.5	0.6	46.90	0.06	57.88	0.02	35	0.28	
93145	139.4042	-3	59.6	41.7	0.1	45.79	0.17	57.81	0.07	28	0.10	*
93146	139.4055	-2	59.6	41.6	0.6	47.59	0.24	57.76	0.12	83	0.03	a
93156	139.4265	-2	59.9	41.6	0.2	45.95	0.08	57.19	0.07	37	-n.d.	
93157	139.4312	-1	59.8	41.8	0.5	45.81	0.04	57.88	0.03	39	0.10	*
93163	139.4433	0	58.6	41.2	0.8	46.78	-.-	58.64	-.-	29	0.09	a
93164	139.4443	-2	59.0	41.1	0.6	45.34	0.04	57.65	0.01	58	0.01	
93174	139.4516	0	59.4	41.5	0.4	45.64	-.-	57.89	-.-	29	-.-	*
93175	139.4582	-1	60.0	42.1	0.5	45.72	-.-	57.83	-.-	34	0.04	*
93184	139.4599	-5	58.9	41.0	0.4	46.52	0.34	57.77	0.06	24	0.37	
93186	139.4586	0	60.0	42.0	0.6	45.82	0.02	57.83	0.01	22	-.-	*
93185	139.4603	-1	59.3	41.4	0.3	47.14	0.19	57.85	0.07	33	0.10	a
93203	139.4720	-6	59.3	41.4	0.6	46.12	0.07	57.73	0.05	67	n.d.	+
93207	139.4730	-1	59.3	41.5	0.6	45.34	-.-	58.05	-.-	24	-.-	
93208	139.4738	-2	59.9	42.0	0.2	45.78	0.11	57.81	0.04	26	0.04	+
93221	139.4844	0	59.7	41.8	1.6	46.84	0.03	57.89	0.02	46	-.-	
93229	139.4889	-1	60.0	42.0	0.3	45.90	0.02	57.88	0.01	34	0.10	+
93237	139.4929	-3	59.6	41.6	0.3	45.91	0.03	57.73	0.02	85	0.05	+
93241	139.4937	-1	59.8	41.7	0.3	46.07	0.14	57.57	0.14	56	0.03	+
93246	139.4993	-3	60.0	41.5	0.5	48.68	0.06	56.89	0.07	32	n.d.	a
93247	139.4996	-2	60.0	42.0	1.0	45.24	0.09	57.73	0.03	41	0.04	
93251	139.5014	0	59.8	41.7	0.8	46.78	-.-	57.52	-.-	30	-.-	
93256	139.5023	0	59.4	41.4	1.4	47.14	-.-	57.63	-.-	35	0.42	
93272	139.5142	-2	59.2	41.3	0.5	46.35	0.05	57.77	0.05	48	-.-	+
93276	139.5173	0	59.3	41.4	0.9	46.83	-.-	57.84	-.-	25	-.-	
93279	139.5212	-2	59.4	41.4	0.2	46.10	0.02	57.74	0.01	56	0.11	+
93282	139.5222	0	59.9	41.7	0.5	45.82	0.11	57.43	0.09	49	0.12	
93283	139.5223	-2	59.4	41.5	0.3	46.15	0.17	58.02	0.13	23	0.24	+
93288	139.5260	-3	59.3	41.3	0.2	45.95	0.08	57.66	0.05	86	0.19	+
93291	139.5300	-2	60.0	42.0	0.3	45.85	-.-	57.68	-.-	23	0.06	+
93292	139.5306	-4	59.3	41.3	0.1	46.32	0.04	57.71	0.03	33	0.15	
annual:												
93101	138.3259	0	59.6	41.9	0.7	43.92	0.28	58.01	0.19	31	0.02	a
93112	138.5297	-2	59.2	41.7	0.5	45.63	-.-	58.43	-.-	89	0.01	a
93299	140.2742	-1	58.8	41.0	0.5	48.77	0.04	58.25	0.01	34	0.07	a
93309	140.3589	-1	59.6	41.8	0.3	49.61	-.-	58.32	-.-	30	0.03	a
93310	140.3850	0	59.8	42.3	0.7	47.12	0.18	59.04	0.09	43	0.01	a
93315	140.4336	-3	59.1	41.3	0.5	47.89	-.-	58.40	-.-	65	0.08	a
93318	140.4421	-3	58.9	41.2	0.5	48.26	0.24	58.39	0.11	31	0.03	a
93324	140.4572	-5	60.1	42.0	0.2	50.11	0.31	57.87	0.08	28	-.-	a

Table 3. (**b**) As (a) for 1994 data (all $Q > 20°$).

#	Ω (J2000) (deg.)	M_v (magn.)	V_g	V_h (km/s)	±	RA_{geo} (deg.)	±	DEC_{geo} (deg.)	±	Q (deg.)	m/C_dS (g/cm^2)	Class.
Aug. 11/12, 1994:												
94101	139.4401	-1	58.9	40.9	0.4	47.96	-.-	58.05	-.-	54	-.-	a
94102	139.4432	0	60.7	42.6	1.2	49.72	-.-	57.03	-.-	60	-.-	a
94104	139.4640	-3	60.1	42.1	0.3	45.07	0.39	57.90	0.32	22	0.15	+
94105	139.4817	-1	59.3	41.3	0.4	46.22	0.25	58.09	0.20	21	-.-	+
94108	139.5108	0	60.2	42.1	0.6	42.07	-.-	58.36	-.-	20	-.-	a
94113	139.5407	-2	60.6	42.5	1.2	46.38	0.20	57.70	0.14	88	-.-	+
94117	139.5573	-3	60.1	42.0	0.3	46.18	0.01	57.84	0.01	51	0.24	+
94119	139.5650	-4	58.8	41.3	0.3	46.30	0.27	58.53	0.22	27	0.03	a
94120	139.5696	-5	-.-	-.-	-.-	45.78	-.-	57.76	-.-	35	-.-	+
94129	139.5836	-7	-.-	-.-	-.-	46.14	0.22	57.75	0.16	32	-.-	+
94136	139.5979	-5	59.0	41.0	0.6	49.55	-.-	57.90	-.-	69	-.-	a
94141	139.6094	-2	-.-	-.-	-.-	43.73	-.-	57.33	-.-	49	-.-	a
94143	139.6111	-2	59.4	41.4	0.4	48.28	0.07	58.68	0.03	85	-.-	a
94147	139.6323	-4	-.-	-.-	-.-	46.50	-.-	57.04	-.-	35	-.-	
annual:												
94148	140.4639	0	59.1	40.8	0.2	52.58	0.07	57.16	0.03	52	0.30	a
94010	140.9932	-1	59.4	42.1	0.2	48.11	0.28	59.52	0.21	38	-.-	a
94020	141.1296	-1	60.2	42.0	0.6	49.71	-.-	57.94	-.-	49	0.18	a
94021	141.1576	-2	60.2	42.2	0.3	48.56	0.13	58.35	0.13	53	-.-	a
94022	141.9310	-1	59.4	41.3	0.4	53.14	-.-	58.14	-.-	23	-.-	a
94024	142.0230	-2	60.3	42.1	0.2	54.44	0.16	58.16	0.05	71	0.03	a
94026	142.0958	-3	59.5	41.9	0.2	51.72	0.03	59.34	0.01	58	0.23	a

radiants of the Nodal Blanket, roughly perpendicular to the ecliptic plane (Fig. 6). 11 out of 16 Filament Perseids are in a circle with 0.27° radius and centred at $RA_{139.5} = 46.0°$, $Dec._{139.5} = +57.7°$ (marked '+' in Table 3). The meteors have a heliocentric velocity $\langle V_h \rangle = 41.59 \pm 0.25$ km s^{-1}, corresponding to orbits with an aphelion close to that of 109P/Swift–Tuttle. There is no gradient with time of encounter (Ω).

The centroid of the dispersion seems to vary from year to year: The 1994 Perseid Filament radiants scatter around $RA_{139.5} = 46.2°$, $Dec._{139.5} = +57.7°$, while the 1991 Perseid Filament data of Shiba et al. (1993) scatter around $RA_{139.5} = 46.1°$, $Dec._{139.5} = +57.5°$. In all years, there was a similar high dispersion and a systematic displacement from the compact cluster of the Nodal Blanket.

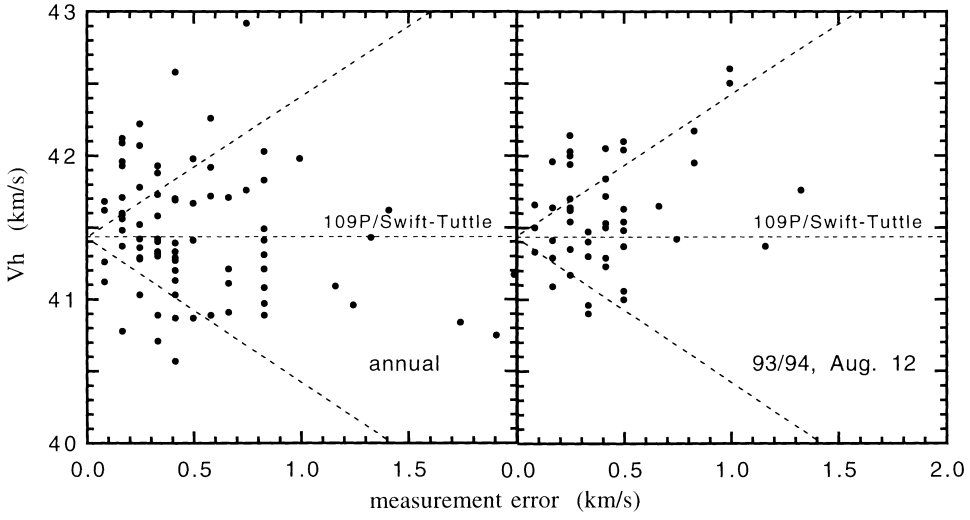

Figure 5. As Fig. 4, for the distribution of heliocentric velocities for annual and outburst Perseids as a function of the estimated measurement error.

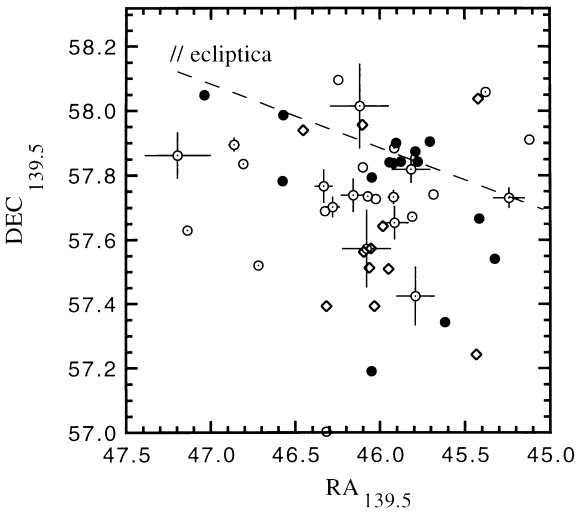

Figure 6. Geocentric radiant position of outburst Perseids in 1993, 1994 and 1991. Symbols indicate Nodal Burst (•), 1993 Filament (⊙), 1994 Filament (○), 1991 Filament (◇, from Shiba et al. 1993). For clarity, error bars are given only for the Filament when measured directly from three-station detections.

4.3 The orbital elements

The four observed parameters (time, RA_{geo}, $Dec._{geo}$, V_g) define the meteor orbit in space. The observed dispersion in radiants translates to significant dispersion in perihelion distance (q), semimajor axis ($1/a$), argument of perihelion (ω) and inclination (I) (Fig. 7). For all data, ω spans a range $\pm 1.9°$, while the inclination covers only $\pm 0.7°$. The dispersion in inclination is $\pm 0.23°$ for the cluster of seven in the Nodal Blanket and $\pm 0.31°$ for the Filament, most of which is accounted for by observational errors.

The small systematic difference in radiant position between the Nodal Blanket and Filament is also manifested in systematic differences in the distribution of orbital elements (Fig. 7). Typically, the Nodal Blanket has 0.2° lower inclination and 0.002 au higher perihelion distance. ω is about the same, while Ω is lower by 0.07°.

Surprisingly, the Perseid Filament orbital elements scatter around the recent 1992 orbit of the comet. Table 4 lists past orbits of 109P/Swift–Tuttle calculated by Yau et al. (1994) and Harris, Yau & Hughes (1995). Dashed lines in Fig. 7 indicate the orbital parameters of the 1992 return. The similarity of the Perseid Filament orbits to the present-day orbit of 109P/Swift–Tuttle implies that comet and meteoroid stream have evolved in much the same way. That is only possible if the distribution of $1/a$ is narrow and peaks at the present value. Indeed, the observed distribution of $1/a$ is consistent with that.

There are small differences between present-day comet orbit and meteoroid stream: The inclination and perihelion distance of the Nodal Blanket are shifted slightly to higher and lower values than the current comet orbit. In both cases, the shift is such as to suggest that the Nodal Blanket is lagging the orbital evolution of the comet, being in between the previous orbit and the present one.

4.4 The density of particles from the measured deceleration

In an attempt to learn more about the morphology of the particles, we have examined the measured deceleration during atmospheric

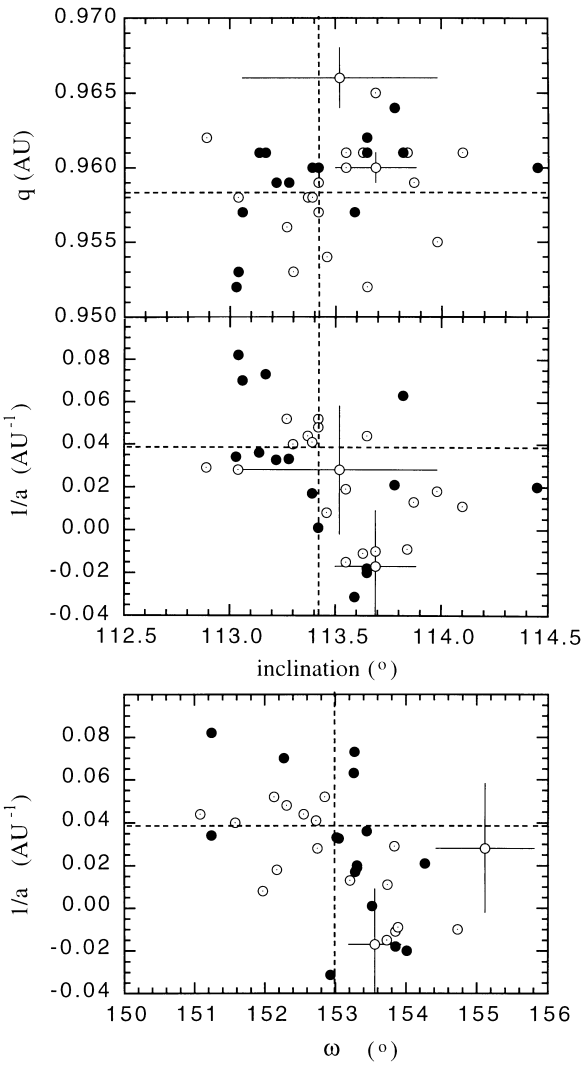

Figure 7. Orbital elements of the radiants shown in Fig. 6 (same symbols). Panels show the inverse semimajor axis ($1/a$), the argument of perihelion (ω), the inclination (I), and the perihelion distance (q). Dashed lines give the orbital elements of the 109P/Swift–Tuttle orbit at the return of 1992 (Yau et al. 1994).

descent. The deceleration (ac) is expected to increase quickly with air density ρ_{air}, whereby ρ_{air}/ac is proportional (in first order, neglecting fragmentation) to the mass-over-surface ratio of the meteoroid (Halliday 1988):

$$m/C_d S = 0.5V^2\rho_{air}/\mathrm{ac}, \quad (3)$$

with V, ac, and ρ_{air} at given altitude. C_d is an unknown drag coefficient, which reflects the shape of the particle. From equation (3), the mass-to-surface ratio can in principle be derived.

$m/C_d\,S$ is measured by fitting a curve of the shape (Ceplecha & Borovicka 1992)

$$V(t)^2 = V_\infty^2 + K\rho(t) \quad (4)$$

to the individual images of the meteor, with $\rho(t)$ the air density at the height of the meteor and V_∞ the pre-atmospheric velocity. Note that V_∞ relates to V_g according to

$$V_g^2 = V_\infty^2 - V_E^2, \quad (5)$$

with the Earth's escape velocity V_E approximately 11.2 km s^{-1}. Transformation to heliocentric velocities V_h includes a correction for the Earth's motion around the Sun and the polar rotation of the Earth. A near-constant m/C_dS is usually found from measured speed and deceleration along the trajectory at various altitudes, suggesting that equation (4) describes the deceleration of the meteor well.

We find that there is no systematic difference in mass-to-surface ratio between Perseids photographed during the outbursts in 1993 and 1994 and the annual Perseids photographed in those years. For the period of the Perseid Nodal Blanket, $m/C_dS = 0.14 \pm 0.12$ ($N = 11$); for the period of the Filament, $m/C_dS = 0.13 \pm 0.11$ ($N = 14$), and, for the annual Perseids, $m/C_dS = 0.10 \pm 0.10$ ($N = 17$).

There is a wide range of values during the outburst as well as during the annual shower. Some of that dispersion is because both end height (H_e) and mass-to-surface ratio depend on the size of the meteoroid. Fig. 8 shows the distribution that results after correction to magnitude zero ($M_v = 0$) meteors according to the dependences

$$H_e(M_v) = 88.7 + 1.7M_v, \quad (6)$$

derived from the observed Perseid trajectories, and

$$m/C_dS(M_v) = m/C_dS(0) \times 10^{-0.13M_v}, \quad (7)$$

which follows from $\log(m) \sim -0.4\ M_v$. We conclude that a magnitude 0 Perseid has $m/C_dS = 0.03$ g cm^{-2} and penetrates to $H_e = 90$ km altitude. In addition, there may be a more compact class of particles with higher m/C_dS. As expected, these denser particles penetrate deeper into the atmosphere, following the increase in atmospheric density with altitude, shown in arbitrary units by a dashed line in Fig. 8. We examined possibly significant deviations from the dashed line between the various dust components, but find no difference between the annual shower and the outburst components. The same is true for the uncorrected values.

We also find no difference in the magnitude-dependent end height of the outburst Perseids compared with those in the annual Perseid shower, and we conclude that our measurements show no evidence that outburst Perseids are more fluffy or more fragile than normal annual Perseid meteoroids.

Table 4. Orbital elements (median values of ensemble) for the three dust components that make up the 1993 (and 1994) Perseid activity and the parent comet P/Swift–Tuttle. Errors give the dispersion, not the error of the median value. The median observational error is given too. Number of orbits: Nodal Blanket (7 – *), 1993 Filament (11 – +), 1994 Filament (6 – +), 1991 Filament (11). Radiants and speed are corrected to Node = 139.5° (J2000).

component	Rageo (J2000)	DECgeo (J2000)	Vg (km/s)	q (AU)	1/a (AU^{-1})	I (°)	ω (°)	π (°)
Nodal Blanket:								
1993 < 139.46	45.88±0.11	57.84±0.04	59.59±0.38	0.9600±0.0016	0.017±0.034	113.39±0.23	153.45±0.58	292.95±0.38
median obs. error	±0.07	±0.03	±0.5	±0.0010	±0.043	±0.32	±0.63	±0.63
Filament:								
1993 >139.46	46.07±0.47	57.73±0.16	59.69±0.29	0.959±0.002	0.028±0.026	113.42±0.24	152.85±0.61	292.37±0.61
median obs. error	±0.04	±0.03	±0.5	±0.001	±0.026	±0.20	±0.39	±0.3
1994	46.14±0.47	57.73±0.37	60.1±0.5	0.963±0.004	0.006±0.032	113.6±0.12	154.3±1.1	293.7±1.1
median obs. error	±0.22	±0.16	±0.5	-.-	-.-	-.-	-.-	-.-
1991 [3]	46.05±0.31	57.56±0.26	-.-	-.-	-.-	-.-	-.-	-.-
1960-1980 [1]	46.8	57.6	59.44	0.953	0.042	113.7	151.7	290.7
Annual stream (corrected to Ω = 139.5)								
DMS (1981-1995)	46.91 ±2.0	57.86±0.9	59.3±0.6	0.953±0.013	0.04±0.043	113.24±1.3	151.5±3.2	292.0±3.3
median obs. error	±0.07	±0.03	±0.5	±0.002	±0.043	±0.44	±0.78	±0.78
IAU (1937-1983)	47.7	58.0	59.48	0.952±0.002	0.027±0.013	113.4±0.1	151.3±0.4	291.2±0.4
109P/Swift-Tuttle:*								
1992 [2]	45.9	57.7	59.41	0.958	0.038	113.4	153.0	292.4
1862 [2]	45.9	57.6	59.44	0.963	0.039	113.6	152.8	292.1
698 [2]	46.0	57.4	59.52	0.973	0.039	113.8	152.9	292.0
-68 [2]	45.9	57.3	59.53	0.981	0.039	113.9	152.4	291.5
-702 [2]	45.7	57.4	59.51	0.973	0.039	113.8	152.5	291.6
-4000 [3]	21	47	61	1.00	0.037	119	151	268
-10000 [3]	0	37	62	1.13	0.022	122	158	256
-20000 [3]	349	32	62	1.54	0.018	123	166	255

* Radiant positions at Earth calculated according to the method of Q adjustment (Hasegawa 1990; Neslusan, Svoren & Porubcan 1998).
[1] Lindblad & Porubčan (1994).
[2] Yau et al. (1994); Marsden et al. (1993).
[3] Harris et al. (1995).

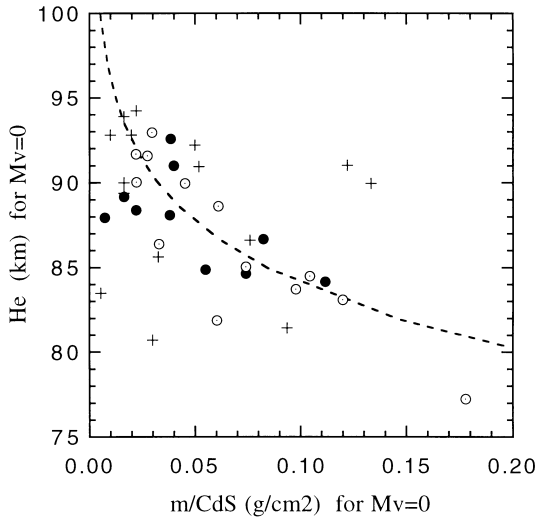

Figure 8. The dependence of the mass-to-surface ratio $m/C_d S$ on the end height of the meteor path (H_e). Symbols as in Fig. 6 with annual shower: +. The dashed line illustrates an atmospheric density gradient dependence.

5 DISCUSSION

Outbursts of Halley-type comets such as 109P/Swift–Tuttle are characteristically of near-comet type, meaning that they only occur when the comet itself returns to perihelion (Jenniskens 1995). We previously reported on a far-comet-type meteor outburst of the α Monocerotid shower, with outbursts at intervals controlled by planetary perturbations. In that case, we were able to prove that these are caused by the wagging trail of a long-period comet (Jenniskens et al. 1997). Near-comet-type outbursts must have a different cause, the most remarkable feature being the concentration of dust near the comet position and lack of outbursts elsewhere along the orbit.

5.1 Recent ejection

Let us first examine whether the features of the Perseid Filament can be caused by the ejection process itself. Both the width of the shower along the node and the radiant dispersion can be indicative of the ejection velocities perpendicular to the plane of the comet orbit, $V_{ej\perp}$.

If the thickness of a ribbon of dust or dust trail (D) represents the maximum excursion of trail particles from the comet orbital plane and the Earth is in the orbital plane, then the corresponding ejection velocity should be (Sykes, Lien & Walker 1990)

$$V_{ej\perp} = V_c \times (0.5D)/r, \quad (8)$$

with V_c the orbital velocity of the comet at the time of emission and r the heliocentric distance of the observer. Note that meteoroid stream width and nodal dispersion $\Delta\Omega$ are related according to (Kresák & Porubčan 1970)

$$D = 2r \tan(\Delta\Omega/2) \sin\epsilon_h, \quad (9)$$

with ϵ_h the angle between the radiant of the heliocentric velocity vector and the Earth's apex and r and D in au. The equivalent duration of the Perseid Filament $\Delta\Omega = 0.058° \pm 0.006$ would imply $V_{ej\perp} \leq 21 \pm 2\,\mathrm{m\,s^{-1}}$ for -1 to $+3$ magnitude Perseids, while the Nodal Blanket would imply $V_{ej\perp} \leq 53 \pm 9\,\mathrm{m\,s^{-1}}$. This is an upper limit, because the expected mass dependence of the duration is not observed.

If the radiant dispersion measures the maximum dispersion of velocity vectors in the plane of the sky resulting from the ejection process, then, to first order, with $V_g = V_h \sin\epsilon_h / \sin\epsilon_g$,

$$V_{ej\perp} = V_g \tan(\Delta\mathrm{Dec.}) \cos(\epsilon_h - \epsilon_g). \quad (10)$$

The smallest radiant dispersion ΔDec. $< 0.03°$ (accounted for by measurement error) was measured perpendicular to the ecliptic plane for the cluster of seven meteoroids of the Perseid Nodal Blanket. This translates to $V_{ej\perp} < 28\,\mathrm{m\,s^{-1}}$ for a -1 magnitude Perseid, in good agreement with the previous estimate. On the other hand, the radiant dispersion in the Perseid Filament (not accounted for by measurement error) would imply ejection velocities $V_{ej\perp} = 100$–$250\,\mathrm{m\,s^{-1}}$, significantly higher.

The dispersion along the comet orbit (the concentration of dust near the comet position) is also a criterion that limits the possible ejection velocity. That extent is determined by the dispersion in semimajor axis (a). The change in semimajor axis during one orbit resulting from ejection velocities parallel to the comet orbit $V_{ej//}$ and the effect of solar radiation forces (β) is described by (Sykes & Walker 1992)

$$\Delta a = \beta a[(1 + e)/(1 - e)] + 2aV_{ej//} \times [(a/GM_0)(1 + e)/(1 - e)]^{1/2}, \quad (11)$$

which translates to $\Delta a = 1.4\times10^3 \beta + 6.7\times10^{-2} V_{ej//}$ ($\mathrm{m\,s^{-1}}$) per orbit. If indeed $\beta = 3\times10^{-4}$ for a typical photographed meteor, then $\Delta a = 0.43 + 6.7\times10^{-2} V_{ej//}$ ($\mathrm{m\,s^{-1}}$), which adds up with every next orbit. The observed dispersion along the comet orbit, $\Delta P/P = 3/2\,\Delta a/a = 1/44$, implies that $\Delta a = 0.4$ au and $V_{ej//}$ is much less than $21\,\mathrm{m\,s^{-1}}$. This assumes that all matter was ejected during the previous return in 1862. In fact, solar radiation forces alone are probably sufficient to disperse the matter as much as observed in a single orbit. A single orbit is not sufficient to account for the large dispersion in radiants of the Perseid Filament. Furthermore, for ejection velocities of $21\,\mathrm{m\,s^{-1}}$ the whole orbit would be filled in a mere 14 orbits, while at 100–$250\,\mathrm{m\,s^{-1}}$ it takes only 2–4 orbits.

We conclude that the ejection process itself can not account for the large radiant dispersion, the lack of correlation between stream duration and meteor brightness (or β) and the concentration of matter near the position of the comet.

5.2 Planetary perturbations and wagging dust trails

One explanation for the rapid increase and decrease of peak rates near the comet position was given by Wu & Williams (1993): planetary perturbations by Jupiter can move the centroid of the dust trail relative to the Earth's orbit. Wu & Williams (1993), Williams & Wu (1994) and subsequent work by Jones & Brown (1996) demonstrated that planetary perturbations can bring the dust trail in and out of the Earth's orbit, thus potentially causing an artificial rapid increase and decrease of peak rates. For assumed ejection velocities V_{ej} approximately $20/r^{1.125}$ $\mathrm{m\,s^{-1}}$, these wagging dust-trail models predict similar series of outbursts back in 1980 (and again around 2004), which are not observed.

Moreover, Jupiter's action on the stream also causes the node to vary, but in an opposite manner to that observed (dash–dotted lines in Fig. 2). These values in Fig. 2 were read off the published figure in Williams & Wu (1994). We note that the Perseid width in the models also varies in synchronization with the location of Jupiter, in contradiction to the observed near-constant width of the stream.

The expected variation of χ with time is not observed. All these features are fundamental flaws in the proposed mechanism.

5.3 Planetary perturbations and protection of the region near the comet position by orbital resonances

Here we propose that near-comet-type outbursts are possible because dust near a Halley-type comet position is protected from close encounters by the planets. This feature goes back to the fundamental difference between Halley-type (i.e. roughly $20 < P < 200$ yr) and long-period (roughly $P > 200$ yr) comets.

Chambers (1997) derived an analytical expression that described this difference between Halley-type and long-period comets. He found that Halley-type comets (and meteoroids) tend to librate around a mean-motion resonance (mostly $1:j$) only out to a certain number j. Hence, we postulate that near-comet-type outbursts are associated with those Halley-type objects that presently librate around mean-motion resonances (usually with Jupiter), or otherwise have not had a recent close encounter with one of the major planets. While the Perseid and Leonid comets fall in this category (both having near-comet-type outbursts), the Lyrid and Aurigid comets do not (both having far-comet-type outbursts).

The Perseid parent librates around the 1:11 resonance with Jupiter. That protects the comet itself from close encounters by Jupiter, but it will also protect the meteoroids in its vicinity from such close encounters. There is a roughly 12-yr window around the position of the comet, not necessary symmetric, that is less strongly affected. In a recent paper, Williams (1997) illustrated such a case of protection by pointing out that the Halley-type Leonid parent 55P/Tempel-Tuttle and the Leonid storm debris are protected from close encounters by Uranus by being close to a 2:5 orbital resonance. In this case, however, Jupiter and Saturn are the dominant perturbers rather than Uranus (Yeomans, Yau & Weissman 1996).

Elsewhere along the Filament, particles move at a range of relative velocities and the debris will be dispersed during a small number of orbits. In this scenario, it is close encounters with Jupiter that remove grains abruptly from the Filament into the annual meteoroid stream. This is consistent with the absence of a significant increase of annual rates in the years that Perseid outbursts were detected. In this light, ejection velocities of $V_{\rm ej} = 600\,{\rm m\,s^{-1}}$ derived from the dispersion of the annual Perseid shower by Harris et al. (1995) are without merit.

The relatively high mass-distribution index in the outburst component may result from the smaller grains dispersing more rapidly along the comet orbit and being more efficiently removed by Jupiter. The dust in the Filament represents only a fraction (some 1/20th) of the large dust grains ejected during the dynamic lifetime of the Filament (i.e. $M > 5 \times 10^{15}$ g). The dynamic lifetime should be of the order of the time-scale for comet 109P/Swift–Tuttle to be locked in an orbital resonance (of order 3×10^3 yr, or about 20 orbits – Chambers 1997). This would place the mass loss in terms of large dust grains at $> 2 \times 10^{14}$ g orbit^{-1}. This value can be compared with an estimate of $> 1.4 \times 10^{14}$ g mass loss during the recent return, from the comet tail modelling by Fulle et al. (1994). If the present-day mass loss is representative of earlier times, then the annual shower was deposited during $< 3 \times 10^4$ yr.

Emel'yanenko & Bailey (1996) pointed out that meteoroid streams in Halley-type orbits tend to remain concentrated in space when the particles librate around mean motion resonances ($1:j$). This may account for the Nodal Blanket. For relatively low ejection velocities, most particles are ejected in orbits that are between the 1:11 and 1:12 orbital resonances. However, some will be trapped in the 1:11 resonance. This matter will evolve in much the same way as the comet, being relatively unaffected by planetary perturbations for a long time. The Nodal Blanket may represent this matter. The sole detection of the Nodal Blanket in 1993 and the narrow radiant dispersion suggests that the Blanket is more confined in semimajor axis than the Perseid Filament, but the larger nodal dispersion and slight difference from the comet orbit suggests a relatively high age.

6 CONCLUSIONS

From photographic and visual observations of recent Perseid outbursts, we conclude the following.

(i) The 'Filament' or 'new peak' (Lindblad & Porubcan 1994) is in fact a ribbon-like structure of dust, here referred to as the 'Perseid Filament', with approximately constant thickness and particle size distribution along the path of the comet.

(ii) An independent dust component was detected in 1993 (and perhaps in 1994), here referred to as the 'Nodal Blanket'.

(iii) The Nodal Blanket includes a cluster of meteoroids with a small dispersion in radiant and speed.

(iv) The Perseid Filament is caused by meteoroids that are significantly dispersed and moving in systematically different orbits from the meteoroids of the Nodal Blanket.

(v) The outburst meteoroids have a wide range in mass-to-surface ratio (density) and do not systematically differ from annual stream meteoroids.

We conclude that the Perseid Filament is not caused by recent ejecta during this or the last return of the comet. Instead, planetary perturbations must have had time to disperse the stream significantly. We rule out the suggestion that low ejection velocities are responsible for the concentration of dust near the comet position: solar radiation forces itself are able to disperse the meteoroids further than observed in a short time-scale. Moreover, we find that the observed variation of the time of maximum is not consistent with the alternative hypothesis that planetary perturbations move a trail of dust temporarily into the path of the Earth.

Instead, we propose that the Perseid Filament (and Nodal Blanket) consists of accumulations of dust from tens of orbits, which have accumulated near the comet position only because that is where the dust is protected from close encounters with Jupiter. Elsewhere, the particles are dispersed into the annual shower debris stream. This protection originates from the comet librating around a 1:11 mean motion resonance with Jupiter. The Nodal Blanket consists of relatively old ejecta with a smaller semimajor axis distribution, and may represent dust that is librating around the same mean-motion resonance as the comet.

The Perseid outbursts remain an interesting target for observational studies in the near future, at least until 2001. Each new outburst will be a unique opportunity to probe the dynamics of large-grain cometary ejecta.

ACKNOWLEDGMENTS

We thank the visual observers that participated in the 1993 Perseid campaign in the South of France, namely Michiel van Vliet, Carl Johannink, Paul Roggemans, Marc de Lignie, Erwin van Ballegoy, Jaap van 't Leven, Robert Haas, Koen Miskotte, Marco Langbroek, Klaas Jobse, Paul van der Veen, Rene-Jan Veldwijk and Mark Olie. Photographic observations were contributed by Andre Kluitenberg,

Ralf Mulder, Jerome van Lier and Romke Schievink. We also thank those who made the 1994 Perseid campaign possible, especially Frank Dibbel and Duncan McNeill of the Fremont Peak Observatory Association. Visual support was given by P. S. Canfield, David Waldbeser, Dora Willoughby, Peter Zerubin, Ingeborg Rice, Lennard Nelson, Ken Lakins, Antony Kent, Randy Thompson and Carroll Borg. There were also individual photographic contributions by David Waldbeser, Kathy Black, Chuck Tribolet, Ted Swift, Kenton R. Parker, Robert C. Madden, P. S. Canfield, B. Nayler and Bob Kuhn. We thank David F. Blake and Friedemann Freund for facilities and encouragement and Marco Fulle for his efforts to help understand the features of the Perseid outbursts. This work is supported by a grant from NASA's Planetary Astronomy program.

REFERENCES

Betlem H., van 't Leven J., Langbroek M., Johannink C., ter Kuile C., 1992, Radiant, 14**,** 143
Betlem H., ter Kuile C.R., van Lignie M., van 't Leven J., Jobse K., Miskotte K., Jenniskens P., 1998, A&AS, 128**,** 179
Brown P., Rendtel J., 1997, Icarus, 124**,** 414
Brown P., Gijssens M., Rendtel J., 1992, WGN, 23**,** 256
Ceplecha Z., Borovicka J., 1992, in Benest D., Froeschle C., eds, Interrelations between Physics and Dynamics for minor Bodies in the Solar System. Edns Frontieres, Gif-sur-Yvette, p. 309
Chambers J.E., 1997, Icarus, 125**,** 32
Davies J.K., Green S.F., Stewart B.C., Meadows A.J., Aumann H.H., 1984, Nat, 309**,** 315
Davies J.K., Sykes M.V., Reach W., Boulanger F., Sibille F., Cesarsky C., 1997, A&A Lett.
de Lignie M., 1993, Radiant, 15**,** 107
Denning W.F., 1898, Astron. Nachr., 148**,** 283
Emel'yanenko V.V., Bailey M.E., 1996, in Asp Conf Ser. Vol. 104. Astron. Soc. Pac., San Francisco, p. 121
Fulle M., Böhm C., Mengoli G., Muzzi F., Orlandi S., Sette G., 1994, A&A, 292**,** 304
Grishchenyuk A., 1993, WGN, 21**,** 283
Halliday I., 1988, Icarus, 76**,** 279
Harris N.W., Yau K.K.C., Hughes D.W., 1995, MNRAS, 273**,** 999
Hasegawa I., 1990, PASJ, 42**,** 175
Hasegawa I., 1993, in Stohl J., Williams I.P., eds, Meteoroids and their Parent Bodies. Slovak Acad. Sci., Bratislava, p. 209
Jenniskens P., 1992, Radiant, 14**,** 55
Jenniskens P., 1994a, A&A, 287**,** 990
Jenniskens P., 1994b, Radiant, 16**,** 93
Jenniskens P., 1995, A&A, 295**,** 206
Jenniskens P., de Betlem H., Lignie M., Langbroek M., 1997, AJ, 479**,** 441
Jones J., Brown P., 1996, in ASP Conf. Ser. Vol. 104. Astron. Soc. Pac., San Francisco, p. 105
Koschack R., Roggemans P., 1991, WGN, 19**,** 87
Kresák L., 1976, Bull. Astron. Inst. Czech., 27**,** 35
Kresák L., 1993, A&A, 279**,** 646
Kresák L., Porubčan V., 1970, BAC, 21**,** 153
Kronk G.W., 1988, Meteor Showers, A Descriptive Catalogue. Enslow, Hillside
Langbroek M., 1993, Radiant, 15**,** 96
Langbroek M., Jennisken, P., 1992, Zenit, July/August 1992**,** 328
Lindblad B.A., Porubčan V., 1994, Planet. Space Sci., 42**,** 117
Lindblad B.A., Simek M., 1986, in Lagerkvist C.I., Lindblad B.A., Rickman H., eds, Asteroids, Comets, Meteors II. Uppsala University, p. 537
Marsden B.G., 1991, IAU Circ. 5330
Marsden B.G., 1992, IAU Circ. 5586
Marsden B.G., Williams G.V., Kronk G.W., Waddington W.G., 1993, Icarus, 105**,** 420
Mason J.W. & Sharp I.D., 1981, J. Br. Astron. Assoc., 91**,** 4
Neslusan L., Svoren J., Porubčan V., 1998, A&A, 331**,** 411
Nogami N., 1995, Earth, Moon, Planets, 68**,** 435
Pin-Xin Xu, 1992. WGN, 20**,** 198
Plavec M., 1955. Bull. Astron. Inst. Czech., 6**,** 20
Rendtel J., 1993, WGN, 21**,** 235
Rendtel J., Arlt R., 1996, WGN, 24**,** 141
Roggemans P., 1989, WGN, 17**,** 127
Roggemans P., Gijssens M., Rendtel J., 1991, WGN, 19**,** 181
Shiba Y., Ohtsuka K., Watanabe J.-I., 1993, in Stohl J., Williams I.P., eds, Meteoroids and their Parent Bodies. Slovak Acad. Sci., Bratislava, p. 189
Shimoda C., Suzuki K., Maeda K., 1993, WGN, 21**,** 130
Sykes M.V., Lebofsky L.A., Hunten D.M., Low F., 1986, Sci, 232**,** 1115
Sykes M.V., Lien D.J., Walker R.G., 1990, Icarus, 86**,** 236
Sykes M.V., Walker R.G., 1992, Icarus, 95**,** 180
Taguchi Y., 1991, Yamamoto Circ. 2170 (in Japanese)
van Vliet M., 1993, Radiant, 15**,** 19
van Vliet M., 1994, Radiant, 16**,** 77
Watanabe J.-I., Tsumura M., Sugawara K., 1990, PASJ, 42**,** L69
Watanabe J.-I., Nakamura T., Tsutsumi M., Tsuda T., 1992, PASJ, 44**,** 677
Williams I.P., 1997, Mnras, 292**,** L37
Williams I.P., Wu Z., 1994, MNRAS, 269**,** 524
Wu Z., Williams I.P., 1993, MNRAS, 264**,** 980
Yau K., Yeomans D., Weissman P., 1994, MNRAS, 266**,** 305
Yeomans D.K., Yau K.K., Weissman P.R., 1996, Icarus, 124**,** 407
Yrjölä I., Jenniskens P., 1998, A&A, 330**,** 739
Znojil V., 1992, WGN, 20**,** 244
Zvolankova J., 1984, Contr. Astron. Obs. Skalnate Pleso, 12**,** 45

This paper has been typeset from a Microsoft Word file prepared by the author.